AIAA 81-4310

Experimental Evaluation of a Perspective Tunnel Display for Three-Dimensional Helicopter Approaches

Arthur J. Grunwald*
Technion—Israel Institute of Technology, Haifa, Israel
and
James B. Robertson† and Jack J. Hatfield‡
NASA Langley Research Center, Hampton, Va.

A computer-generated perspective tunnel display for a steep and strongly curved three-dimensional helicopter approach is studied. The necessary control variables for following a curved trajectory are analyzed, the effectiveness of superimposed predictor symbology is investigated, and a suitable predictor law is formulated. The theoretical considerations are validated by an extensive fixed-base simulator program. The tunnel display with a superimposed predictor symbol is shown to outperform conventional-type displays in its abilities to follow a curved trajectory in the presence of gust disturbances, to enter the trajectory from an unknown position outside this trajectory, as well as to monitor automatic approaches. The feasibility of the tunnel display for operation in actual flight has been demonstrated in an exploratory flight test.

Nomenclature

a_l, a_v = component of inertial acceleration in y_b and z_b axis directions, respectively, m/s^2
cov( ) = autocovariance
D = predictor distance, m
d_l, d_v = lateral or vertical deviation from the trajectory, m
d_ψ = lateral intercept angle of vehicle axis and trajectory direction, rad
k_{pv} = adjustment gain for vertical predictor distance
R_l, R_v = radius of the lateral or vertical vehicle path, m
s = Laplace operator
sc( ) = deviation score for entry maneuvers, m
T_p = prediction time, s
T_{sl}, T_{sv} = lateral or vertical settling time, s
t = time, s
v, w = component of $\vec{V}$ in y_b and z_b axis directions, respectively, m/s
$\vec{V}, V$ = vehicle velocity vector and magnitude, respectively, m/s
x_b, y_b, z_b = body axis coordinate system
$\delta_b, \delta_c, \delta_s, \delta_r$ = pitch, collective, roll, and yaw control commands, respectively, cm
ϵ_l, ϵ_v = lateral or vertical predicted deviation, m
ψ, θ, ϕ = yaw, pitch, and roll attitude angles, respectively, rad

Introduction

THE excessive workload present in the conventional helicopter instrument approach to landing and the advent of microprocessor and cathode ray tube (CRT) technology have led to the development of computer-generated pictorial displays. With these displays, the control information is presented in an integrated format, derived from the "through-the-windshield" visual field geometry. Various formats of electronic pictorial displays for the straight approach to landing have been proposed and experimentally evaluated by Van Houtte,[1] Wilckens,[2] Murphy and Greif,[3] and Steinmetz et al.[4] However, in these references, the need for predictive information has not been recognized. Roscoe and Eisele[5] propose a detailed contact-analog straight approach-to-landing display which includes superimposed predictor symbology, but do not analyze or evaluate the display experimentally. Pictorial displays for moderately curved approach trajectories have been proposed by Knox and Leavitt[6] describing a path-in-the-sky contact analog display and by Adams and Lallman[7] using the perspective image of a box for displaying displacement as well as command information. However, in these references the effect of the forcing function of strongly curved trajectories has not been investigated or evaluated.

Pictorial displays, which proved successful in straight approaches, are suitable in particular for defining complicated curved trajectories. With the "tunnel display" format, chosen in this study and first proposed by Wilckens for straight approaches[2], the three-dimensional approach path is displayed as a winding and descending "tunnel in the sky," which combines both preview of the trajectory as well as the necessary control information in one display format. Apart from gust disturbances, the trajectory curvature constitutes the main forcing function to the pilot-vehicle system and is responsible for a large part of the pilot activity.

A difficulty, which is not recognized in the referenced previous work, is that pictorial displays cannot fully reconstruct the visual field since the peripheral vision is partially missing. It is shown in previous work[8,9] that in visual field control, vital rate cues providing the system damping are derived from the peripheral vision, so that with pictorial displays the damping is expected to be impaired. In this paper, it is shown analytically and experimentally that a predictor symbol, well adjusted to the control task, is able to fulfill the dual function of furnishing the system with the necessary damping cues, as well as providing the correct control information for following strongly curved trajectories. On the other hand, the tunnel image provides the positional and directional orientation with respect to the trajectory. The tunnel, combined with the superimposed predictor, emerges in this study as a successful display combination in which the tunnel image compensates for predictor deficiencies and the predictor compensates for the lack of damping cues.

Received May 10, 1980; revision received Dec. 12, 1980.

*Senior Lecturer Control Systems Engineering, Dept. of Aeronautical Engineering.
†Aerospace Scientist, Flight Electronics Division.
‡Aerospace Technologist, Flight Electronics Division.

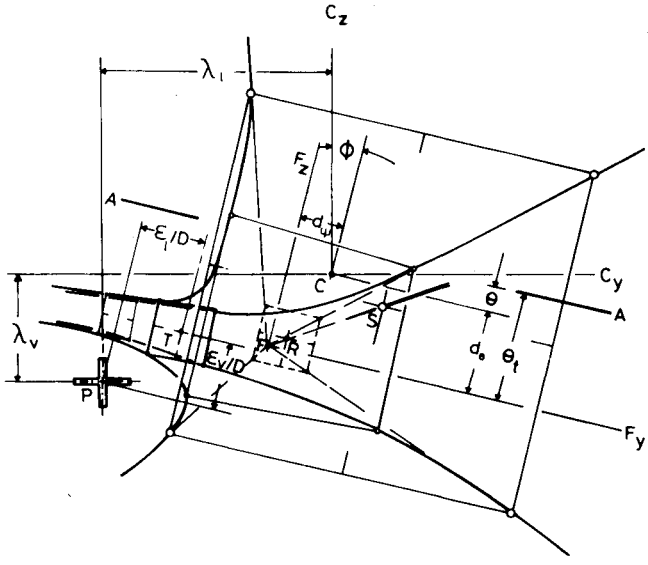

Fig. 1a Positional, rate, and directional cues derived from the tunnel display.

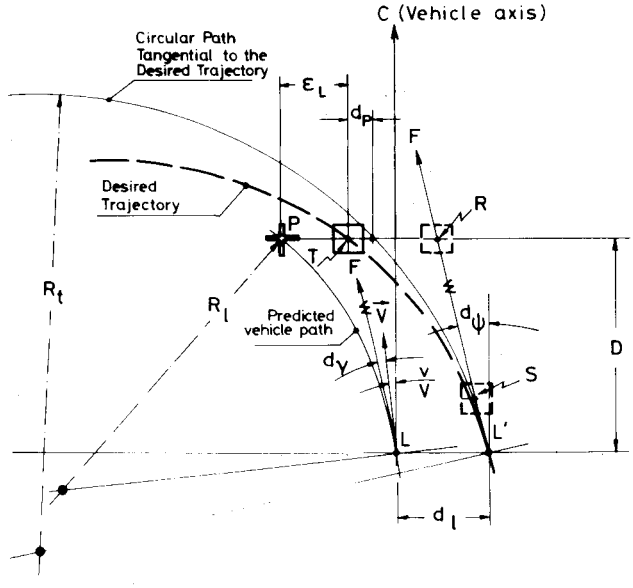

Fig. 1b Horizontal situation of Fig. 1a.

Theoretical Background

Vehicle Model

A linear time-invariant model of a CH-47 tandem-rotor helicopter is used. The longitudinal and lateral dynamics are assumed to be fully decoupled. The flight is nominally straight and level with a constant forward velocity of $V = 33.5$ m/s (110 ft/s). The vehicle is augmented with a lateral stability augmentation system (SAS) providing directional stability and turn coordination and a longitudinal SAS providing longitudinal stability and keeping the forward velocity constant. The vehicle dynamics and SAS are given in Ref. 11.

Basic Geometry of the Perspective Tunnel Display

The basic geometry by which control cues are derived from the tunnel display is shown in Fig. 1a. The desired trajectory is presented by the perspective image of a tunnel. Line AA in this image represents the horizon, being parallel to the "through-the-windshield" true horizon. The vehicle is banked to the left and the bank angle ϕ follows from the inclination of line AA with respect to the display monitor reference frame. Point C indicates the center of the image and represents the vehicle axis. Point C is not explicitly displayed, but can be estimated by the pilot by using the monitor frame as a reference. Point F, which is also not explicitly displayed, indicates the instantaneous desired trajectory direction and can be estimated by the pilot by extending the four tunnel corner lines nearest to the vehicle to a focal point at infinity. Point S is the center of the nearest square and is to be estimated as well. The imaginary centerline FS provides the lateral and vertical positional information. When defining the F_y axis to be parallel and F_z axis to be perpendicular to the horizon, the lateral and vertical deviations of the vehicle from the trajectory can be estimated from the distance between F and S in the F_y and F_z directions, respectively. The vehicle attitude with respect to the tunnel can be estimated from the deviation of focal point F from the center of the image C. Thus, the lateral intercept angle d_ψ of the vehicle axis with the instantaneous tunnel direction is estimated from the distance between F and C in the F_y direction, and the vertical intercept angle d_θ is estimated from the distance between F and C in the F_z direction. The downslope of the trajectory θ_t follows from the depression of point F below the horizon line AA. Rate cues may originate from the rate of change of the above-mentioned quantities. An impression of forward motion is derived from the "passing by" of tunnel segments. Preview of the trajectory to be followed is obtained by considering a centerpoint T on the trajectory, a distance D ahead of the vehicle. Point R is a point on centerline FS and a distance D ahead as well. Unlike R, which is to be estimated, the tunnel section at T is explicitly shown. The distance between T and R in the F_y direction provides an indication of the trajectory curvature, while the distance between T and R in the F_z direction indicates changes in the vertical downslope.

The variables, necessary for generating the tunnel image, are the x_i, y_i, and z_i inertial coordinates of the vehicle position, as well as the yaw, pitch, and roll attitude angles of the vehicle, ψ, θ, and ϕ, respectively.

The Predicted Vehicle Position

It is shown in Refs. 8 and 9 that, in visual field control, essential lateral rate and acceleration cues are obtained from the future vehicle path, which is estimated from the pattern of velocity vectors in the visual field. In this process the peripheral vision is utilized in particular. Since, due to the limited size of the monitor, the peripheral vision is partially missing, this estimation process in particular is expected to be noisy.

A way of restoring the information lost in the peripheral vision is to display the predicted vehicle position explicitly on the tunnel image, as shown in Fig. 1. The predicted vehicle path is based on the assumption that the vehicle proceeds from the present moment onward into the future with constant lateral (in y_b body axis direction) and vertical (in z_b body axis direction) inertial accelerations, which are equal to the momentary lateral and vertical accelerations, $a_l(t)$ and $a_v(t)$, respectively. Thus, the projections of the predicted vehicle path on the horizontal plane of the vehicle ($x_b y_b$ plane) and on the vertical plane of symmetry of the vehicle ($x_b z_b$ plane) are circular and tangential to the vehicle velocity vector $\vec{V}$. The lateral and vertical path radii follow from

$$R_l(t) = V^2/a_l(t) \qquad R_v(t) = V^2/a_v(t) \tag{1}$$

where V is the forward velocity. The predictor symbol P indicates a point on the vehicle path, a distance D ahead of the vehicle. When defining C_y and C_z as the lateral and vertical monitor axes (see Fig. 1a), the deviations of P from the center of the monitor in the C_y and C_z directions are given by

$$\lambda_l = \frac{v}{V} + \frac{(D/R_l)}{1+\sqrt{1-(D/R_l)^2}} \qquad \lambda_v = \frac{w}{V} + \frac{(D/R_v)}{1+\sqrt{1-(D/R_v)^2}} \tag{2}$$

where R_l and R_v follow from Eqs. (1) and v and w are the components of $\vec{V}$ in y_b and z_b directions, respectively. λ_l and λ_v are in fractional screen coordinates (screen limits are $+1$ and -1), for a $+45$ to -45 deg horizontal and vertical field of view. It follows from Eqs. (1) and (2) that the only variables necessary to display the predictor symbol are the vehicle velocity V, velocity components v and w, as well as the inertial accelerations a_l and a_v.

A valid control strategy for the tunnel-and-predictor display is to minimize the error between predictor P and tunnel section T. The ratio D/V constitutes the prediction time $T_p = D/V$ s ahead of the vehicle. It is clear that a correct value of T_p is vital in obtaining a satisfactory overall system performance. Control theoretical considerations in the choice of T_p are discussed hereafter.

Predictor Analysis

The horizontal situation in Fig. 1b shows the circular predicted vehicle path with radius $R_l(t)$, which is tangential to $\vec{V}$ at the actual vehicle position L, the arbitrarily curved desired trajectory, and a circular path tangential to the desired trajectory at point L', with radius $R_t(t)$ corresponding to the momentary trajectory curvature at L'. The lateral deviation from the trajectory is denoted by d_l and the intercept angle of velocity vector and trajectory direction by d_γ. For small deviations, d_l and d_γ satisfy

$$\frac{\partial d_\gamma}{\partial t} = \left(\frac{V}{R_l(t)} - \frac{V}{R_t(t)}\right) \qquad \frac{\partial d_l}{\partial t} = V d_\gamma(t) \tag{3}$$

When defining the lateral control error ϵ_l as the distance between predicted vehicle position P and desired position T, both at distance D ahead, it follows from the geometry of Fig. 1b that for small d_l, d_γ, and D/R_t, the following linearized expression for ϵ_l can be derived

$$\epsilon_l(t) = d_l(t) + D d_\gamma(t) + \frac{D^2}{2}\left(\frac{1}{R_l(t)} - \frac{1}{R_t(t)}\right) + d_p(t) \tag{4}$$

or with Eqs. (3) and after Laplace transformation,

$$\epsilon_l(s) = (1 + T_p s + \tfrac{1}{2} T_p^2 s^2) d_l(s) + d_p(s) \tag{5}$$

where the term d_p constitutes a preview of the trajectory and accounts for changes in curvature. For straight trajectories or for trajectories with a constant curvature, d_p will be zero. Equation (5) shows that by using ϵ_l as the lateral control error, the open-loop transfer function is furnished with a pair of complex zeros with a fixed damping factor of $\xi = 0.707$, and a natural frequency which can be adjusted to the requirements of the system by adjustment of T_p. Since the vehicle transfer function for the lateral displacement, given in the Appendix, is dominated by three poles close to the origin, the zeros of Eq. (5) will be vital in stabilizing the system. The prediction time T_p should be chosen such that it yields the best compromise between positional accuracy and system damping for the given vehicle dynamics and airspeed.

A second important property of the control error ϵ_l is that it yields a zero steady state value of d_l in following straight trajectories or trajectories with a constant curvature, as can be seen by setting ϵ_l and d_p to zero in Eq. (5).

The vertical control error ϵ_v can be formulated in a way similar to the lateral one. However, the vehicle transfer function for the vertical displacement d_v, given in the Appendix, is effectively of a lower order than the one for the lateral displacement, which requires less rate information to stabilize the system. Therefore, a value of T_p which is satisfactory for the lateral control will probably yield a sluggish vertical response and will cause rapid vertical predictor motions. The vertical prediction time can be adjusted to a smaller value by replacing D in Eq. (2), by $D' = k_{pv} D$, where k_{pv} is a gain between 0 and 1.

Predictor-and-Square Display

It is suggested earlier that for a well-chosen prediction time T_p, control can be accomplished by minimizing the error between predictor P and tunnel section T (see Fig. 1a). For this control task, a display which would show only the predictor-cross and the tunnel-section square would be sufficient. The control task then deteriorates into a simple flight-director tracking task, which can be carried out with existing electromechanical instrumentation. However, this "predictor-and-square" display yields the following shortcomings:

1) Since the pilot is forced to use the control error between cross and square, system performance might be impaired if the predictor does not provide the correct information, e.g., as the result of a wrongly adjusted prediction time T_p or of errors in the estimation of the variables which are used to drive the predictor.

2) The predictor-and-square display is limited to situations where the square is within the field of view. In case the square moves outside the field of view, the display provides no control information other than the polarity of the control error, which seriously impairs system performance.

Experimental Validation

Description of the Experimental System

The experimental simulator program was carried out at the Langley Research Center Real-Time Simulation Facilities. A CDC Cyber 175 computer was used on a time-sharing basis for the real-time digital simulation of the CH-47 helicopter dynamics. The computed vehicle motions were imparted to an AGT 130 Adage Graphics terminal which generated images of the various display configurations. These images were displayed in a fixed-base general aviation simulator cabin, and used by the pilot-subject to generate the control commands, which in turn were imparted to the Cyber computer.

The simulator cabin was equipped with a two-axis spring-loaded viscous-damped control stick, spring-loaded rudder pedals, and an unloaded balanced collective control lever. A forward stick motion δ_b generated a forward velocity command, a lateral stick motion δ_s a roll-rate command, and a collective lever motion δ_c a vertical velocity command. In order to obtain turn coordination, the differential cyclic command δ_r was controlled by the SAS, so the rudder pedals were not used. All control information was derived from two display monitors, measuring 33 cm (13 in.) and 22.9 cm (9 in.) diagonally. The average distance from the subject's eye to the monitor was about 75 cm (30 in.).

The actual flight testing was carried out at the Flight Display Research System at Wallops Island, Va. A description of this system is given in Ref. 10. A fully instrumented CH-47 research helicopter served as the flight vehicle. Display images were generated by a ground-based AGT 130 graphics terminal, scan converted, transferred to the vehicle by TV video link, and displayed in the cockpit. The necessary variables for generating the display were derived from a ground-based laser tracker measuring the vehicle position, as well as from on-board sensor data telemetered to the ground-based system.

Display Configurations

The following display configurations were investigated.

1) Basic tunnel display (see Fig. 2a): The tunnel has a constant and square cross section of width 45.72 m (150 ft), which corresponds to the width of a typical runway. The tunnel squares (1) are 91.44 m (300 ft) apart and the interconnecting line segments (2) are 15.4 m (50 ft) long. Every second segment is omitted. Only the five squares nearest to the vehicle are drawn. The tunnel is shown in the viewing range of 0-762 m. The maximum horizontal and vertical field

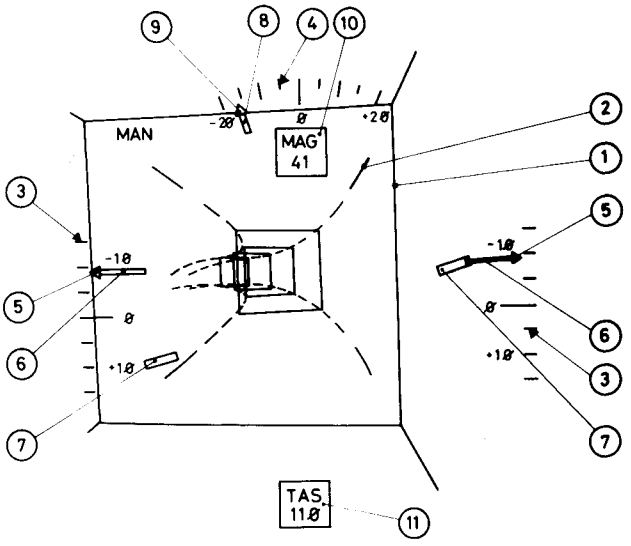

Fig. 2a Basic tunnel display, roll-stabilized version.

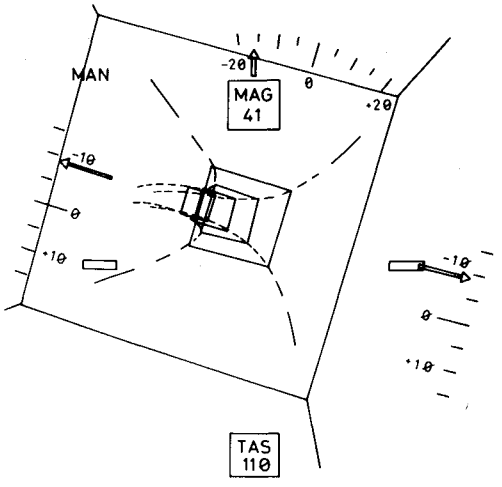

Fig. 2b Basic tunnel display, roll version.

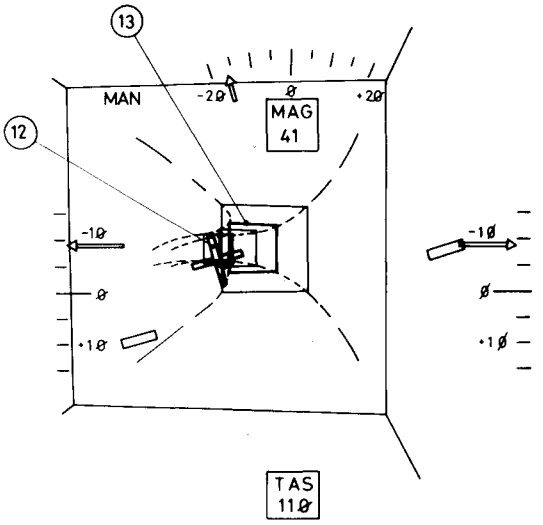

Fig. 2c Tunnel display with superimposed predictor symbol.

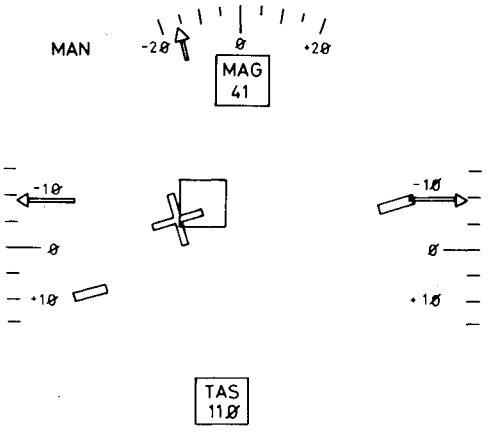

Fig. 2d Predictor-and-square display.

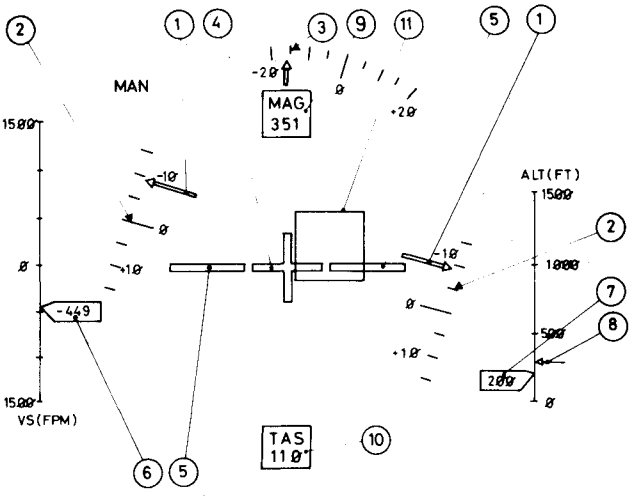

Fig. 2e Electronic attitude director indicator with vertical speed indicator and altimeter.

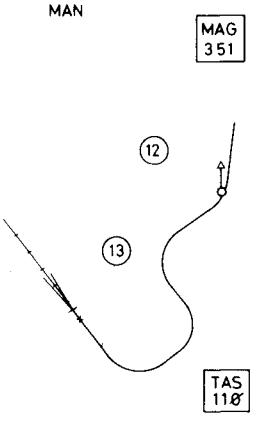

Fig. 2f Horizontal situation indicator.

of view is from +45 to −45 deg. At the left and right side of the image are located the pitch scales (3), and at the top of the image the roll scale (4). The pitch pointers (5) are attached to the partially visible horizon bar (6). The pitch motion is visualized by a vertical displacement of the tunnel image and horizon bar, while the pitch scales remain vertically fixed.

In visualizing the roll motion, two versions are considered. In the first version (Fig. 2a) the tunnel image, horizon, and pitch and roll scales are roll stabilized and the bank angle ϕ is visualized by rotating aircraft reference symbology, which would indicate the wing line (7) and vertical stabilizer (8) with the roll pointer (9) in fixed-wing aircraft. In this case, the image is not conformal with the through-the-windshield visual field and can be used only in head-down-type displays. In the second version (Fig. 2b), the tunnel image together with pitch and roll scales is rotated and the aircraft reference symbology remains stationary.

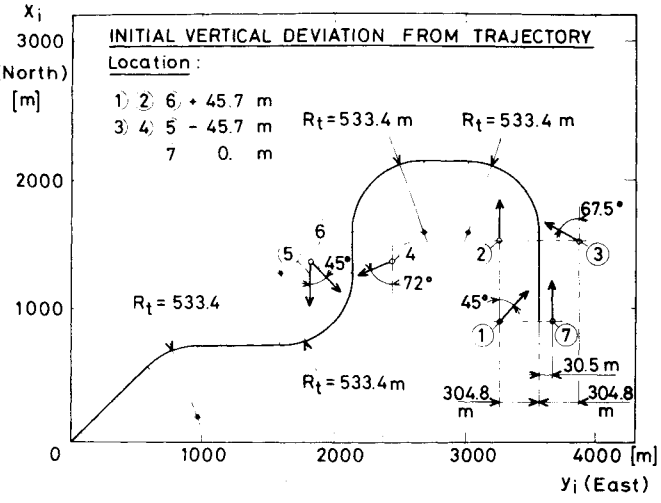

Fig. 3a Plan view of the desired trajectory.

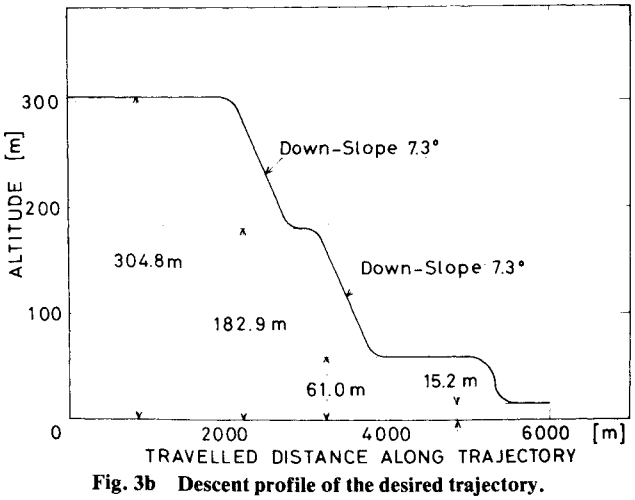

Fig. 3b Descent profile of the desired trajectory.

Magnetic heading (MAG) ⑩ and true airspeed (TAS) ⑪ are displayed digitally on the vertical centerline at the top and bottom of the image, respectively (see Fig. 2a).

2) Tunnel display with superimposed predictor symbol (see Fig. 2c): This configuration is identical with configuration 1 on which is superimposed a reference cross ⑫ symbolizing the predicted vehicle position at distance D ahead of the vehicle and a bright square ⑬, which is the cross section of the tunnel at distance D symbolizing the desired future vehicle position. In contrast with the squares of the tunnel structure, this square moves along with the vehicle at a fixed distance D ahead. The outer dimensions of cross and square are equal, i.e., of width 45.72 m (150 ft). The cross remains parallel to the wing line.

3) Predictor-and-square display (see Fig. 2): This configuration is identical with configuration 2, in which the tunnel image is omitted and only the predictor cross and tunnel square are displayed.

4) Electronic attitude director indicator (EADI) with horizontal situation indicator (HSI): This configuration serves as a baseline for comparing conventional with more advanced display concepts. On the upper monitor the EADI display of Fig. 2e is shown, with horizon bar ①, pitch scales ②, roll scale ③, fixed vehicle axis reference cross ④, wing line ⑤, vertical speed indicator ⑥, actual altitude ⑦, commanded altitude ⑧, and digital readouts of magnetic heading ⑨ and true airspeed ⑩. In addition to this, the actual lateral and vertical deviation is visualized by a displacement of the square ⑪. A displacement of the square, equal to its width, corresponds to a deviation of 45.7 m (150 ft). On the lower monitor (Fig. 2f) the horizontal situation is shown with vehicle reference symbol ⑫ which remains stationary and a moving map ⑬ which shows a plan view of the desired trajectory.

Description of the Experiments

All experiments were concerned with the approach to landing in a range 4500-150 m from the landing site. A plan view of the desired trajectory is shown in Fig. 3a and the desired vertical descent profile along the trajectory is shown in Fig. 3b. In all experiments the forward velocity was kept constant at 33.53 m/s (110 ft/s). The following experiments were performed:

1) Manual following of the trajectory in the presence of random lateral and vertical atmospheric disturbances: The pilot was instructed to minimize the lateral and vertical deviations from the trajectory with minimum control effort. The atmospheric disturbances were modeled by first-order filtered band-limited Gaussian white noise with a break frequency of 0.2 rad/s. The rms value of the lateral disturbances was 5.33 m/s and of the vertical disturbances 4.57 m/s. Each run started from initial location 7 (see Fig. 3a) and lasted 120 s, during which the means and autocovariances of deviations, vehicle motions, and control commands were computed.

2) Entering the trajectory from a randomly chosen, unknown location outside the trajectory: The pilot was instructed to enter the trajectory as rapidly and smoothly as possible with minimum control effort. Each run started randomly from one of the six initial locations shown in Fig. 3a, with an initial lateral deviation of 304.8 m (1000 ft) and an initial vertical deviation of 45.7 m (150 ft). Atmospheric disturbances were not present in this experiment. In order to prevent the pilot from knowing his initial position and thus prevent him from planning his entry beforehand, the display was initially blanked until the start of a simulation run. Each entry lasted 50 s, during which the following performance scores were computed: a) the lateral settling time T_{sl}, defined as the time from the start of the run to the moment the lateral deviation settles within a ± 15.24 m (50 ft) tolerance about the desired trajectory, and the vertical settling time T_{sv}, for which the settling tolerance is ± 10.67 m (35 ft); b) the autocovariances of vehicle motions and control commands; c) the lateral deviation score, defined as

$$\mathrm{sc}(d_l) = \frac{1}{T_2 - T_1} \int_{t=T_1}^{T_2} |d_l| \, dt \tag{6}$$

where $T_1 = 10$ s and $T_2 = 50$ s. The vertical deviation score was computed in the same way with $T_1 = 6$ s and $T_2 = 50$ s. T_1 is chosen to be about 25% less than the best possible settling time.

3) Monitoring experiments: Each run started as an automatic flight. At a randomly chosen instant, a failure occurred in the automatic control system, chosen randomly from four possible failures, such as: a) lock-on control commands, b) biases in sensor data used to drive the predictor, c) turn-coordination failure due to a biased rudder input, and d) roll-damping failure. The pilot was instructed to detect the failure, to engage the manual control mode, and to bring the vehicle back onto the desired trajectory. Measured were the time needed by the pilot to detect the failure, the time needed for manual recovery, as well as overall error scores. A more detailed description of the experiment is given in Ref. 11.

Results

Four subjects participated in the experimental validation program. Subjects 1 and 2 were general aviation research pilots with 5200 and 2200 h of flight experience, respectively, of which 20 and 30% was in helicopters, respectively. Both

Table 1 Results of the trajectory-following experiment

	Trajectory Following Experiment, Subject 3										
	Basic Tunnel, No Roll	EADI + Map	Tunnel + Predictor, k_{pv} = 0.2, D = 228.6 m (750 ft)		Tunnel + Predictor, No Roll, k_{pv} = 1.				Predictor Square, No Roll, k_{pv} = 1.		
			No Roll	Roll	D = 91.4 m (300 ft)	D=137.2 m (450 ft)	D=228.6 m (750 ft)	D=304.8 m (1000 ft)	D = 91.4 m (300 ft)	D=228.6 m (750 ft)	D=304.8 m (1000 ft)
No. of Runs	7	10	6	6	4	5	5	8	5	5	4
cov(d_ℓ) [m²]	578.6* ±320.5**	3,663.8 ±2,687.5	100.0 ± 12.3	114.8 ± 23.7	49.2 ± 5.7	68.2 ± 3.7	107.3 ± 26.7	173.6 ± 39.6	67.0 ± 4.1	138.1 ± 48.5	276.3 ± 41.3
cov(d_v) [m²]	205.8 ±141.7	1,089.8 ± 746.7	28.2 ± 13.6	37.8 ± 10.4	11.9 ± 1.5	17.4 ± 4.2	59.2 ± 40.8	46.4 ± 17.7	12.9 ± 2.4	53.9 ± 10.5	71.0 ± 10.7
cov(ε_ℓ) [m²]	NR***	NR	146.3 ± 27.6	209.8 ± 67.3	37.4 ± 6.9	60.7 ± 4.7	260.2 ± 47.7	937.5 ± 102.2	62.1 ± 4.8	229.1 ± 54.7	515.4 ± 91.7
cov(ε_v) [m²]	NR	NR	100.0 ± 29.5	137.7 ± 59.2	23.2 ± 2.2	41.0 ± 11.2	250.3 ± 88.5	1,289.0 ± 566.2	22.0 ± 2.7	302.2 ± 34.0	1,036.2 ± 129.4
cov($\dot{\varepsilon}_\ell$) [(m/sec)²]	NR	NR	251.4 ± 17.1	223.3 ± 20.6	13.4 ± 0.8	64.5 ± 19.6	380.7 ± 87.4	1,080.0 ± 442.8	18.2 ± 3.7	437.5 ± 146.4	694.8 ± 236.5
cov($\dot{\varepsilon}_v$) [(m/sec)²]	NR	NR	112.2 ± 13.7	117.0 ± 18.5	23.8 ±30.0	160.0 ±300.0	2,121.7 ±1,719.3	14,963.7 ±4,250.6	91.6 ± 8.0	4,897.7 ±3,190.0	12,159.1 ±1,654.0
cov(d_ψ) [10^{-3}rad²]	11.7 ± 3.1	51.4 ± 21.7	4.33 ± 0.55	4.52 ± 1.23	3.69 ± 0.46	4.40 ± 0.29	4.67 ± 1.53	6.98 ± 1.11	5.04 ± 0.46	4.86 ± 1.85	5.74 ± 1.05
cov(p) [10^{-3} (rad/sec)²]	8.12 ± 2.78	7.71 ± 3.89	2.51 ± 0.33	2.27 ± 0.31	3.58 ± 0.37	2.44 ± 0.24	2.24 ± 0.46	1.48 ± 0.37	4.39 ± 0.44	1.57 ± 0.19	0.89 ± 0.16
cov(δ_s) [cm²] (Roll)	2.66 ± 0.70	2.76 ± 1.29	1.61 ± 0.18	1.30 ± 0.23	1.68 ± 0.14	1.37 ± 0.07	1.36 ± 0.24	1.03 ± 0.20	1.79 ± 0.14	1.09 ± 0.08	0.71 ± 0.16
cov(δ_c) [cm²] (Collective)	10.53 ± 4.10	6.23 ± 2.59	6.67 ± 2.32	7.60 ± 4.00	5.50 ± 0.27	4.02 ± 0.68	5.59 ± 1.07	4.92 ± 1.00	5.32 ± 0.56	4.37 ± 0.39	5.54 ± 1.86

* Average of n runs. ** Standard deviation of n runs. *** Not relevant for this display configuration.

subjects had extensive simulator experience as well. Subject 3, an engineering physicist, had about 400 h of flight experience of which 15% was in helicopters. Subject 4, an aeronautical engineer, had no actual flight experience, but had an extensive fixed-base simulator background.

During two to four simulator sessions of 1-3 h duration each, the subjects familiarized themselves with the various display configurations. In addition to this, prior to the production runs, 3-12 training runs were made for each experimental condition.

Significance tests on the difference between averages were performed with a Student-T-test at a 5% level of significance. Although significant differences between the results of the four subjects were observed, the general trends of these resulta were rather similar. Thus, within the limited scope of this paper, only the most characteristic results of subject 3 are presented.

Results of the Trajectory-Following Experiment

The basic tunnel display enabled a markedly better tunnel-following accuracy and better system damping than the EADI-and-map display, as can be seen from the significantly lower autocovariances of deviations d_l and d_v and intercept angle d_ψ (see Table 1).

The tunnel-and-predictor yielded significantly smaller deviations and a smaller roll activity than the basic tunnel display (see Table 1), indicating that system damping and following accuracy greatly improve with the addition of a predictor symbol. This fully supports the theoretical assumptions that the predictor is able to restore the essential damping cues, which were lacking as a result of the impaired peripheral vision.

The effect of the predictor distance D for the tunnel-and-predictor display is shown in Fig. 4. With increasing D, deviations were found to increase strongly, whereas the roll activity was found to decrease strongly. At D=91.4 m (300 ft) the system lacks damping, and at D=304.8 m (1000 ft) the system is too inaccurate. The optimum predictor distance for lateral control, for this control task and airspeed, tends to be in the range of 137.2-228.6 m (450-750 ft), which corresponds to a prediction time of 4-7 s. However, for the vertical control, this predictor distance resulted in a sluggish response and in disturbingly rapid vertical predictor motions. The vertical prediction time was reduced by adjustment of gain k_{pv}, which was chosen such that the autocovariances of the vertical and lateral error rates, $\dot{\epsilon}_v$ and $\dot{\epsilon}_l$, were about the same. A value of k_{pv}=0.2 yielded acceptable predictor motions and a satisfactory vertical response.

The performances of the tunnel-and-predictor and of the predictor-and-square, are compared in Fig. 4. For predictor distances away from the optimum, the tunnel-and-predictor yielded significantly smaller deviations than the predictor-and-square. However, for the tunnel-and-predictor the covariance of the lateral error ϵ_l was found to be significantly larger (see Table 1). This indicates that for an incorrectly adjusted predictor, the pilot relies on the tunnel image rather than on the error between the predictor and the square and thus the tunnel image compensates for predictor deficiencies.

In this fixed-base simulator study, no significant difference between the roll version and roll-stabilized version was found (see Table 1). However, the presence of motion cues is expected to augment this difference.

Results of the Trajectory-Entry Experiment

The entry experiment was conducted in a series of six runs. For each run the initial location was chosen at random and without replacement from the set of six initial locations given in Fig. 3a. The results of the six runs in each series were averaged in order to obtain the series scores.

For the basic tunnel, the deviation scores, settling times, and roll-activity were found to be significantly smaller than for the EADI-and-map display, indicating a faster, more accurate, and better damped entry (see Table 2). The effect of adding a predictor symbol to the basic tunnel is noticed in a markedly lower roll activity, as well as in significantly lower deviation scores and settling times (see Table 2).

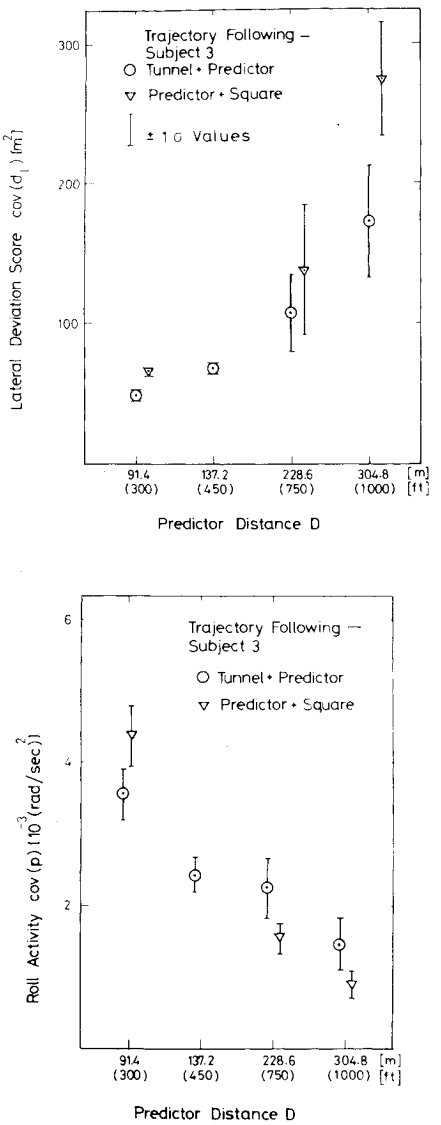

Fig. 4 Results of the trajectory-following experiment: the effect of *D* on the lateral deviation score and on the roll activity.

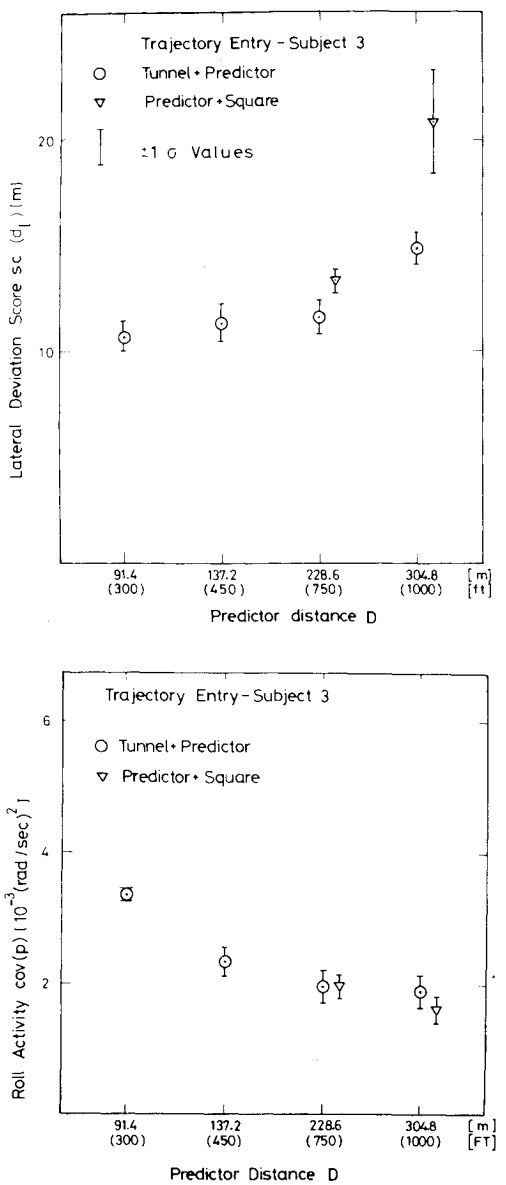

Fig. 5 Results of the trajectory-entry experiment: the effect of *D* on the lateral deviation score and on the roll activity.

For the tunnel-and-predictor, deviation scores and settling times were found to increase strongly with *D*, while the roll activity was found to decrease strongly with *D* (see Fig. 5). Thus, also for the entry experiment, the optimum *D* tends to be in the range of 137.2-228.6 m, or 4-7 s prediction time.

In the entry experiment the predictor-and-square display was ineffective for predictor distances smaller than 228.6 m (750 ft), since the tunnel square was out of the visible range during the first part of the entry. For larger than optimal *D* the tunnel and predictor yielded significantly smaller deviation scores and settling times, while the predicted deviations were significantly larger, indicating that the pilot used the tunnel image rather than the predictor (see Table 2).

No significant difference was found between the entry scores of the roll version and roll-stabilized version (Table 2).

Results of the Monitoring Experiment

In the monitoring experiment the tunnel-and-predictor, the predictor-and-square and the EADI-and-map display were investigated. The results, given in Ref. 11, show that the tunnel-and-predictor display yielded significantly smaller failure detection times and manual recovery times than the two other displays. The EADI-and-map display yielded the worst performance, with significantly larger overall error scores.

Results of the Exploratory Flight Test

Due to limitations in flight time, only the roll version of the tunnel-and-predictor display was investigated. Unfortunately, not all of the variables required for displaying the predictor symbol were available. Due to these predictor deficiencies and, to a larger extent, due to the lack of a forward-velocity hold system, the flight control task was considerably more demanding than the simulator task and the workload rather high. Subject 1 (the research pilot) commented that, in spite of the task difficulty, the display was acceptable and provided sufficient information for following the trajectory. The lateral deviations from the trajectory remained within about ±50 m.

Conclusions

1) The perspective tunnel image provides adequate positional and directional information and yields a markedly better accuracy in trajectory following and trajectory entry than the conventional EADI-and-map display.

2) The basic tunnel display yields a poor system damping due to the lack of rate information caused by the narrow visual field. A predictor symbol superimposed on the tunnel image restores the lacking rate information, which is essential for an adequately damped system.

Table 2 Results of the trajectory-entry experiment

Trajectory Entry Experiment, Subject 3									
	Basic Tunnel, Roll	EADI + Map	Tunnel + Predictor Roll, k_{pv}=0.2 D=137.2 m (450 ft)	Tunnel + Predictor, No Roll, k_{pv} = 0.2				Predictor + Square No Roll, k_{pv} = 0.2	
				D = 91.4 m (300 ft)	D=137.2 m (450 ft)	D=228.6 m (750 ft)	D=304.8 m (1000 ft)	D=228.6 m (750 ft)	D=304.8 m (1000 ft)
No. of Series of 6 Entries	4*	5	4	4	4	4	4	4	4
sc(d_l) [m]	19.4 ± 2.1	34.4 ± 3.0	12.1 ± 1.0	10.8 ± 0.6	11.4 ± 0.9	11.7 ± 0.7	14.8 ± 0.8	13.3 ± 0.5	20.8 ± 2.5
sc(d_v) [m]	6.9 ± 0.4	19.1 ± 1.6	3.3 ± 0.2	3.0 ± 0.2	3.6 ± 0.2	4.8 ± 0.3	4.7 ± 0.5	5.7 ± 0.2	7.2 ± 0.5
Ts_l [sec]	28.3 ± 5.6	46.5 ± 2.9	17.1 ± 1.4	16.3 ± 0.6	16.8 ± 1.0	16.2 ± 0.4	22.1 ± 4.0	23.4 ± 1.4	36.0 ± 1.3
Ts_v [sec]	31.3 ± 2.1	44.6 ± 2.3	10.6 ± 0.2	10.2 ± 0.5	10.5 ± 0.6	12.9 ± 2.3	14.6 ± 2.4	18.1 ± 1.7	24.2 ± 3.7
cov(ε_l) [10 m^2]	NR	NR	47.9 ± 1.9	64.0 ± 1.3	48.0 ± 1.1	21.6 ± 0.5	17.0 ± 2.0	20.3 ± 0.5	11.1 ± 3.5
cov(ε_v) [10^{2}m^2]	NR	NR	0.94 ± 0.06	1.20 ± 0.10	0.91 ± 0.04	0.80 ± 0.06	1.30 ± 0.20	1.17 ± 0.14	0.91 ± 0.19
cov($\dot{\varepsilon}_l$) [10^2 (m/sec)^2]	NR	NR	0.99 ± 0.04	1.03 ± 0.03	0.94 ± 0.04	1.17 ± 0.18	2.64 ± 0.88	1.11 ± 0.07	2.56 ± 0.67
cov($\dot{\varepsilon}_v$) [10^2 (m/sec)^2]	NR	NR	0.20 ± 0.04	0.09 ± 0.01	0.22 0.01	0.91 ± 0.33	1.96 ± 0.38	0.97 ± 0.63	2.97 ± 0.69
cov(p) [10^{-3} (rad/sec)^2]	6.02 ± 1.55	9.40 ± 2.36	2.72 ± 0.33	3.39 ± 0.15	2.37 ± 0.23	1.96 ± 0.27	1.91 ± 0.23	1.96 ± 0.15	1.57 ± 0.17
cov(δ_B) [cm^2] (Roll)	1.94 ± 0.48	3.15 ± 0.73	1.15 ± 0.12	1.26 ± 0.05	0.94 ± 0.09	0.85 ± 0.10	0.81 ± 0.09	0.86 ± 0.06	0.70 ± 0.05
cov(δ_C) [cm^2] (Collective)	5.69 ± 0.75	4.39 ± 1.71	2.52 ± 0.10	2.92 ± 0.10	2.72 ± 0.05	2.46 ± 0.04	2.50 ± 0.21	2.21 ± 0.09	2.08 ± 0.06

* 4 × 6 = 24 entries total for this configuration.

3) For the given vehicle dynamics and forward velocity of 33.5 m/s (110 ft/s), a predictor symbol which predicts the vehicle position 4-7 s in advance yields the best compromise between positional accuracy and system damping for lateral control. However, for the vertical control this prediction time yields too rapid vertical predictor motions. A vertical prediction time of 20% of the lateral one yields the best pilot acceptance.

4) The flight-director type of predictor-and-square display, with a well-adjusted predictor, performs equally well as the tunnel-and-predictor display in trajectory following. However, performance of the predictor-and-square display degrades strongly with a badly adjusted predictor or in situations in which the tunnel cross-section square is out of the visible range.

5) The roll version and roll-stabilized version of the tunnel display perform equally well in trajectory following and entry. The roll version should be chosen in head-up displays in which the image has to conform to the visual world.

6) The tunnel-and-predictor display performs very satisfactorily in the detection and manual recovery of failures in automatic flight.

Appendix

Transfer functions for the linearized lateral and vertical displacements for nominally straight and level flight at V=33.5 m/s with SAS engaged are derived in Ref. 11 and are given by

$$H_{\delta_s}^{d_l}(s) = k_{d_l} \frac{[s+0.23][s+2.14][s^2+2(0.43)(0.25)s+(0.25)^2][s^2+2(0.013)(3.52)s+(3.52)^2]}{s^2[s+0.007][s+0.21][s+2.36][s+2.77][s^2+2(0.42)(0.32)s+(0.32)^2]} \tag{A1}$$

and

$$H_{\delta_c}^{d_v}(s) = k_{d_v} \frac{[s+11.28][s^2+2(0.76)(0.63)s+(0.63)^2]}{s[s+0.46][s+11.16][s^2+2(0.67)(0.73)s+(0.73)^2]} \tag{A2}$$

respectively.

Acknowledgments

The authors wish to express their appreciation to NASA Research pilots Tomas Edwards and Perry Deal for their contributions as pilot subjects, as well as for their valuable comments. The research was carried out at Langley Research Center, Hampton, Va., during a National Research Council Associateship of Arthur J. Grunwald from 1977-1979.

References

[1]Van Houtte, N.A.J., "A Perspective Glideslope Indicating System," *6th Annual Conference on Manual Control,* April 1970, pp. 117-131.

[2]Wilckens, V., "New Aspects in Man/Machine-Integration; Recommendations for Research Priorities," *9th Annual Conference on Manual Control,* May 1973.

[3]Murphy, M.R. and Greif, R.K., "Simulator Evaluation of a Perspective Clipped-Pole Display and Trust-Vector Controller for VTOL Zero-Zero Landings," *11th Annual Conference on Manual Control,* May 1975, pp. 268-283.

[4]Steinmetz, G.G., Morello, S.A., Knox, C.E., and Person, L.E. Jr., "A Piloted-Simulation Evaluation of Two Electronic Display Formats for Approach and Landing," NASA TN-D-8183, April 1976.

[5]Roscoe, S.N. and Eisele, J.E., "Integrated Computer-Generated Cockpit Displays," International Symposium on Monitoring Behaviour and Supervisory Control, Berchtesgaden, West Germany, March 1976, *NATO Conference Series III, Human Factors,* Vol. 1, Plenum Press, New York, 1976, pp. 39-49.

[6]Knox, C.E. and Leavitt, J., "Description of Path-in-the-Sky Contact Analog Piloting Display," NASA TM-74057, 1977.

[7]Adams, J.J. and Lallman, F.J., "Description and Preliminary Studies of a Computer Drawn Instrument Landing Approach Display," NASA TM-78771, Nov. 1978.

[8]Grunwald, A.J. and Merhav, S.J., "Vehicular Control by Visual Field Cues; Analytical Model and Experimental Validation," *IEEE Transactions on Systems, Man, and Cybernetics,* Vol. 6, No. 12, 1976, pp. 835-845.

[9]Grunwald, A.J. and Merhav, S.J., "Effectiveness of Basic Display Augmentation in Vehicular Control by Visual Field Cues," *IEEE Transactions on Systems, Man, and Cybernetics,* Vol. 8, Sept. 1978, pp. 679-690.

[10]Hatfield, J.J., Elkins, H.C., Batson, V.M., and Poole, W.L., "A Flexible Flight Display Research System Using a Ground-Based Interactive Graphics Terminal," *Applications of Computer Graphics in Engineering,* NASA SP-390, Oct. 1975, Paper 20.

[11]Grunwald, A.J., "An Experimental Evaluation of an Electronic Perspective Tunnel Display for 3-D Helicopter Approach-to-Landing," Technion Aeronautical Engineering Rept. TAE 383, Technion, Haifa, Israel, Oct. 1979.